Published in final edited form as:
Biomed Microdevices. 2009 December ; 11(6): 1205–1212. doi:10.1007/s10544-009-9338-0.

Cell encapsulation and oxygenation in nanoporous microcontainers

Barjor Gimi[1,2], **Joonbum Kwon**[2], **Li Liu**[1], **Yang Su**[1], **Krishnamurthy Nemani**[1], **Krutarth Trivedi**[2], **Yonghao Cui**[2], **Behroze Vachha**[1], **Ralph Mason**[1], **Wenchuang Hu**[2], and **Jeong-Bong Lee**[2]

Barjor Gimi: barjorg@yahoo.com; Joonbum Kwon: ; Li Liu: ; Yang Su: ; Krishnamurthy Nemani: ; Krutarth Trivedi: ; Yonghao Cui: ; Behroze Vachha: ; Ralph Mason: ; Wenchuang Hu: ; Jeong-Bong Lee:

[1] UT Southwestern Medical Center at Dallas, 5323 Harry Hines Blvd, Dallas, TX 75390, USA

[2] The University of Texas at Dallas, 800 West Campbell Road, Richardson, TX 75080-3021, USA

Abstract

With strides in stem cell biology, cell engineering and molecular therapy, the transplantation of cells to produce therapeutic molecules endogenously is an attractive and achievable alternative to the use of exogenous drugs. The encapsulation of such cell transplants in semi-permeable, nanoporous constructs is often required to protect them from immune attack and to prevent their proliferation in the host. However, effective graft immunoisolation has been mostly elusive owing to the absence of a high-throughput method to create precisely controlled, high-aspect-ratio nanopores. To address the clinical need for effective cell encapsulation and immunoisolation, we devised a biocompatible cell-encapsulating microcontainer and a method to create highly anisotropic nanopores in the micro-container's surface. To evaluate the efficacy of these nanopores in oxygenating the encapsulated cells, we engineered 9L rat glioma cells to bioluminesce under hypoxic conditions. The methods described above should aid in evaluating the long term survival and efficacy of cellular grafts.

Keywords

Microencapsulation; Nanoporosity; Cell therapy; Cell encapsulation therapy; Immunoprotection; Immunoisolation

1 Introduction

Cell transplantation is an alternative to administering exogenous drugs. Cells can produce biotherapeutic material in direct and timely response to host pathophysiology; cells are potentially a perennial and regenerative source of therapy. The transplantation of cells may have utility in the therapy of several diseases including Type I diabetes (Desai et al. 1998; King 2001; Shapiro et al. 2000), CNS malignancies (Bjerkvig et al. 2003; Visted et al. 2001), hypoparathyroidism (Hasse et al. 2000) and hemophilia (Hortelano et al. 1996), while eliminating the need for donor organs and the associated surgical complications. However, cell xeno- and allo-transplantation requires a lifelong dependence on immunosuppressant drugs with attendant risks of infection and the increased risk of cancer (de Groot et al. 2004; Vial and Descotes 2003).

Correspondence to: Barjor Gimi, barjorg@yahoo.com.

To eliminate or reduce the use of immunosuppressant drugs, cells are encapsulated in an immunoisolative semi-permeable space that allows the transport of nutrients, waste products and biotherapeutic molecules while prohibiting the passage of large molecules of the immune system (Rihova 2000). Current strategies in encapsulated cell therapy face numerous challenges including i) the lack of precise control over capsule nanoporosity and ii) the inadequate oxygenation of encapsulated cells. To address these challenges, we devised small cell-encapsulating microcontainers with precise control over surface nanoporosity that may have utility in cell based xeno- and allo-graft therapy. We engineered cells to report on their oxygenation status post encapsulation.

We used photolithography to fabricate an epoxy-based, SU-8, microcontainer for cell encapsulation, and developed a method for the rapid formation of highly anisotropic nanopores within the surface of the microcontainer using a combined strategy of electron beam lithography (EBL) and oblique-angle metal deposition. This approach to nanopore formation represents a significant advance in the high aspect ratio, high-throughput formation of nanopores, providing an avenue for the translational and clinical use of such microcontainers for cell therapy.

To ascertain the viability and oxygenation of encapsulated cells, we created a cell line that is constitutively fluorescent and that generates bioluminescent signal under hypoxic conditions. We transfected 9L rat glioma cells to express the bioluminescent protein luciferase under the hypoxia response element (HRE) promoter, and transduced these cells with a retrovirus so as to constitutively express green fluorescent protein (GFP). The resultant 9L-3HRE-luc/GFP cells were imaged with fluorescence imaging (FLI) and bioluminescence imaging (BLI) in normoxic and hypoxic conditions, and signal intensity was correlated with cell number. Cell fluorescence was used as a marker of cell viability and cell number within the transparent microcontainers while the bioluminescence signal, produced under hypoxic conditions, reported on the oxygenation status of the encapsulated cells. This imaging strategy may prove critical in assessing and optimizing the *in vivo* efficacy of cell encapsulation because encapsulated cells may report ‘normal’ survival and function while suffering from hypoxia. Our imaging strategy may be easily adapted for a variety of cell lines used in cell therapy.

2 Methods

Microcontainer fabrication

The microcontainer has two discrete components, 1) a hollow cubic base that is loaded with cells, and 2) a lid that closes the microcontainer after it is filled with its cellular payload (Fig. 1(a–d)).

The SU-8 hollow cubic base comprises a 50 μm thick bottom face, and four 200 μm thick side walls on which a 50 μm ‘female’ structure is patterned to accommodate a corresponding ‘male’ structure formed in the lid. To create this cubic base, first a 50 μm thick SU-8 2025 (Microchem, Newton, MA) photoresist layer was spun on a Pyrex wafer. This SU-8 layer was patterned to form the bottom face of the hollowed cubic base. Next, 200 μm thick SU-8 2075 was spun, patterned and baked to form the four side walls of the hollowed cubic base. This 200 μm thick SU-8 layer was not photodeveloped to ensure uniform thickness of the next layer -50 μm thick SU-8 2025 which was patterned to form the female structure. The fabrication sequence for the hollowed cubic base is shown in Fig. 2.

The SU-8 lid comprises a 100 μm thick rectangle for structural integrity, and a 35 μm male structure that interfaces with the female structure in the cubic base. Recessed within the lid is a matrix of cylindrical wells with a thin, semi-permeable nanoporous SU-8 membrane at the base of the wells. The thin membrane was devised to permit rapid and selective molecular

transport. The lid fabrication was started with the deposition of a 4,000 Å Cr adhesion layer by electron beam evaporation. 2,000 Å thick Cr alignment marks were formed on top of the Cr coated wafer using a lift-off process. 350 nm thin SU-8 2000.5 was then spun and patterned to form the thin membrane for the formation of the nanopore arrays. Next, 70 nm PMMA A2 photoresist was spun on the patterned 350 nm thin membrane and baked. The nanopore arrays were formed on the PMMA A2 layer by EBL using a 30 kV applied voltage, a 120 pA current and a 0.9 nC line dose. For each lid, 16 arrays of 1,680 nanopores, each of 1 μm length, were formed. To protect this patterned PMMA A2 during the etch process, 200 Å thick Al was deposited on the top and side walls using oblique-angle metal deposition. The 350 nm thin SU-8 membrane was etched by O_2 plasma in reactive ion etch (RIE). The Al protection layer was then removed with Al etchant and the PMMA A2 layer was removed by acetone. This process resulted in the formation of very deep nanopores while retaining a small feature size and uniform cross section. Next, 100 μm thick SU-8 2075 was spun and patterned to form the main rectangular structure of the lid. 35 μm thick SU-8 2025 was then spun and patterned to form male structure on the periphery. Finally, the SU-8 lids were released from the wafer substrate using Cr wet etchant. The fabrication sequence for the microcontainer lid is shown in Fig. 3. Non-porous lids, without nanopores and wells, were similarly fabricated for control experiments.

Characterization of microcontainers and of membrane porosity

The cubic bases and lids of the microcontainer were coated with 20 Å Cr, imaged with a scanning electron microscope (SEM) and analyzed for structural integrity, uniformity, and dimensions. SEM images of the nanoporous membrane were separately and similarly imaged. The nanopore width was measured for 12 nanopores chosen at random. Nanopore length was measured using Adobe Photoshop software (www.adobe.com).

To characterize IgG transport through the nanoporous lid, we loaded a microcontainer with FITC-conjugated IgG (20 mg/ml; www.sigma.com), closed the microcontainer with the nanoporous lid and placed it in 100 μl PBS in a 96-well plate. An open microcontainer filled with FITC-conjugated IgG and no lid was placed in 100 μl PBS in a second well. A third well was filled with 100 μl PBS for background correction. Fluorescence measurements were performed on the liquid from each well absent the micro-containers using a fluorescence microplate reader.

9L-3HRE-luc/GFP cell transfection, transduction and culture

9L rat glioma cells were grown in Dulbecco's Modified Eagle Medium (DMEM; Mediatech, Inc, Herndon, VA) supplemented with 10% fetal bovine serum (FBS; Hyclone, Logan, Utah) and antibiotics (100 units/ml penicillin and streptomycin, Mediatech, Inc, Herndon, VA). 3×10^5 9L cells were transfected with 2 μg of the 3HRE-tk-LUC vector (Tian et al. 1997) using the FuGENE 6 transfection reagent (Roche Diagnostics, Indianapolis, IN) and selected by highest expression of the luc gene using 400 μg/ml G-418 disulfate (RPI, Research Products Inc, Mt. Prospect, IL) under simulated hypoxia. The stable clones were then transduced with a GFP retrovirus (Invitrogen, www.invitrogen.com) and selected using 10 μg/ml puromycin dihydrochloride (Sigma, St. Louis, MO). The resultant 9L-3HRE-luc/GFP cells were cultured in DMEM and supplemented with 200 μg/ml G418 and 3 μg/ml puromycin. All cell counts presented in this study were performed with a hemocytometer and using Trypan blue exclusion.

2.1 *In vitro* characterization of FLI and BLI signal from 9L-3HRE-luc/GFP cells in culture

Cell preparation—9L-3HRE-luc/GFP cells were seeded in two clear bottom, black, 96-well tissue culture plates (www.bdbiosciences.com) and maintained overnight in DMEM supplemented with 10% FBS + Penn/Strep + Gluc. Cells were seeded with 5,000, 10,000, 25,000, 50,000 and 100,000 cells per well and in triplicate. The cells observed under hypoxia

were incubated with 100 μl DMEM containing 0.2% FBS and supplemented with 100 μM $CoCl_2$ (Wang et al. 2000); 100 μl of DMEM supplemented with 0.2% FBS was added to the 'normoxia' wells. The plates were incubated for 4 h and 24 h at 37°C and 5% CO_2. After incubation, the cells were washed twice in PBS and the medium in the wells was replaced with i)100 μl of PBS for 'normoxia' wells, and ii) 100 μM $CoCl_2$ in 100 μl of PBS for 'hypoxia' wells. The plates were then imaged using FLI and BLI. One row of cells from both the normoxia and the hypoxia conditions were recovered by trypsin digestion and were counted using a hemocytometer and Trypan blue exclusion. Additionally, 9L-3HRE-luc/GFP cells (2,500, 5,000, 7,500, 10,000, 25,000, 50,000 and 100,000) were suspended in PBS supplemented with 0.2% FBS in a 96-well plate. Fluorescence was measured with λ_{ex} 495 nm and λ_{em} 530 nm using a Spectramax M5 fluorescence microplate reader (Molecular Devices, www.moleculardevices.com).

FLI and BLI—The 96 well plate was imaged using a Xenogen IVIS Spectrum system (www.caliperls.com). First fluorescence images were acquired to capture GFP signal with a 465 nm excitation wavelength and a 520 nm emission wavelength using 1 s exposure. Then, 10 μl (i.e. 400 μg/well) of *D*-Luciferin (Biosynth AG®. Biochemica & Syntetica, Switzerland) was added to each well and bioluminescence images were acquired using 30 s exposure.

Image Analysis—FLI and BLI signal intensities were quantified as the photons/sec (p/s) using Living Image 3.0 software (www.caliperls.com).

Statistics—Given the limited sample size, statistical analyses were performed using the non-parametric exact Wilcoxon rank sum test with statistical software (SAS/STAT, version 9.1.2, 2004, SAS system for Windows, SAS Institute, Cary, NC), where $p<0.05$ was considered significant.

Hypoxia response of 9L-3HRE-luc/GFP cells encapsulated within the microcontainers—To ascertain the post encapsulation oxygenation status of the 9L-3HRE-luc/GFP cells, we encapsulated a spheroid cluster of ~3,000 cells within the cubic bases of the microcontainers that were then closed with either 1) the nanoporous lids (n=6), or 2) the non-porous lids (n=6). The microcontainers were placed in a 100 mm Falcon tissue culture dish (www.bdbiosciences.com). Next, liquid extracellular matrix (ECM) gel, kept at 4°C, was pipetted atop the closed devices, and the tissue culture dish was incubated for 30 min for the gel to polymerize and ensure that the lids and microcontainers were secured in place. Then 15 ml of DMEM supplemented with FBS + Penn/Strep + Gluc was added to the tissue culture dish. Unencapsulated cell clusters were kept as controls in a separate dish under identical conditions. After 48 h incubation at 37°C to permit hypoxic conditions, the microcontainers' lids were dislodged and the tissue culture dishes were imaged using BLI with 30 s exposure.

3 Results

Microcontainer characterization

The microcontainer base structures remained anchored to the wafer substrate after fabrication, autoclaving, cell loading and lid attachment (>98% yield) and the lids were easy to handle and place on the base structures using microforceps. There was a good mate between the male and female structures of the lid and base, respectively that closed the microcontainer. Scanning electron microscope (SEM) imaging showed structural uniformity for both the cubic base and the lid, and that the thin membrane within the lid remained intact after the fabrication and lift-off process. The assembled microcontainers were easily dissociated from the wafer using microforceps, when necessary for experimental purposes.

Characterization of microcontainers and of membrane porosity

Nanopores were formed in the thin SU-8 membrane of the lid using a combined strategy of EBL and oblique-angle metal deposition. SEM assessment of the reverse side of the membrane showed that the nanopores penetrated through the thin SU-8 membrane (Fig. 1(c)) while maintaining their dimensional fidelity; we were able to achieve nanopores ranging from 20 nm to 80 nm width (Fig. 1(d)). The nanopore width for the devices used in our experiments was 23.84±2.78 nm (mean ± sd). The rectangular nanopore length was 0.93±0.014 μm (mean ± sd).

IgG-FITC fluorescence observed in the supernatant of open microcontainers was 96.744 RFU whereas that from the nanoporous microcontainer was 18.606 RFU, background corrected.

3.1 *In vitro* FLI and BLI of 9L-3HRE-luc/GFP cells in culture

FLI of cells in culture—Fluorescence using the microplate reader showed a positive correlation between cell number and fluorescence intensity over the entire range of 2,500–100,000 cells (Table 1). Fluorescence intensity per cell was $2.28\times10^{-4}\pm7.1\times10^{-5}$ RFU (mean ± sd).

FLI at the 4 h time point showed that FLI signal intensity positively correlated with cell number seeded regardless of whether the cells were maintained in standard culture medium or in medium treated with $CoCl_2$ to chemically simulate hypoxia (Fig. 4). To demonstrate correlation between FLI signal intensity and cell number, we counted cells from ‘normoxia’ wells at the 24 h time point and normalized the FLI signal to cells counted. Fluorescence intensity per cell was 144.69±33.6 p/s for the wells seeded with 10,000–100,000 cells.

BLI of cells in culture—BLI signal from cells maintained under hypoxic conditions was significantly higher than that from cells maintained under normoxic conditions after 24 h, for all cell numbers ($p<0.05$, one-tailed exact Wilcoxon rank sum test) except for 5,000 cells where the BLI signal was higher for the hypoxia condition as compared with normoxia, but statistical significance was not obtained.

At the 4 h time point, the ratio of fluorescence to bioluminescence intensities was 22.86±4.8 for ‘normoxia’ and 11.05±5.7 for ‘hypoxia’.

3.2 Hypoxia response of 9L-3HRE-luc/GFP cells encapsulated within the microcontainers

9L-3HRE-luc/GFP cells encapsulated within microcontainers with non-porous lids yielded more BLI signal (17.3×10^4p/s) than microcontainers with nanoporous lids (1.04×10^4p/s) after 48 h, although the difference was not statistically significant as determined by a one-tailed exact Wilcoxon rank sum test. BLI revealed no signal from unencapsulated controls.

4 Discussion

We have fabricated a biocompatible (Cho et al. 2008; Voskerician et al. 2003), nanoporous microcontainer that could be utilized for encapsulating and delivering cells for cell therapy. The microcontainers are optically transparent to enable the visualization of cells post encapsulation (Fig. 5). The small size of the microcontainers, which can easily be further miniaturized, should facilitate the delivery of cellular grafts to currently difficult-to-access highly vascularized sites within the host (Burgos et al. 2006; Gimi et al. 2009; Kin et al. 2002). To protect the cellular graft from stresses during transplantation, a key failure mode in many encapsulation schemes, we used the mechanically robust epoxy-based polymer, SU-8, which is characterized by a tensile strength of 60 MPa and a Young’s modulus of 2 GPa (www.microchem.com). The high yield of reproducible microcontainers should enable the

large graft volumes that are needed for successful transplantation in applications such as the transplantation of pancreatic islets for type 1 diabetes therapy (Shapiro et al. 2000).

A key feature of the nanofabrication strategy presented here is the high throughput creation of high aspect ratio nanopores in SU-8 that are characterized by their small feature size (20 nm). The nanoporous membrane, in conjunction with the small size and 250 × 250 × 250 μm^3 encapsulation volume of the microcontainer were devised to facilitate the rapid bi-directional transport of ions and small molecules and the oxygenation of the encapsulated cells (Thomlinson and Gray 1955). The ability to precisely control the width of the nanopores should enable their fine-tuning to permit the free transport of nutrients and cellular products while immunoprotecting the cellular graft by preventing the entry of large molecules of the immune system into the microcontainer. An important advantage of excluding immune molecules from the graft is that cellular transplants can potentially be studied in immunocompetent animals, thereby providing a superior representation of the human system.

SEM imaging showed integrity of the thin SU-8 membrane in the microcontainer lid. SEM images of the nanopores showed a uniform cross-sectional profile. Together, these results indicate that our strategy results in the creation of deep, anisotropic, uniform nanopores within the surface of our cell encapsulation device. The thin, nanoporous membrane minimizes the molecular transition time across it, and should aid in rapid cellular response to secretagogues (Chicheportiche and Reach 1988). Our use of EBL and oblique-angle metal deposition for the creation of these nanopores resulted in more than three orders of magnitude increase in the speed of nanopore formation over the use of a focused ion beam (FIB) and represents the possibility for the widespread use of our devices in the translational and clinical application of cellular grafts. Furthermore, the scheme for creating deep nanopores while maintaining feature size may aid in the inactivation of complement molecules upon passage through these nanopores, thereby facilitating graft survival and function (Iwata et al. 1995). As observed in our membrane porosity experiment, IgG transport is severely impeded by the nanoporous membrane. However, it may be necessary to improve membrane architecture. We will hone our fabrication approach to include the serial application of low-dose E-beams as opposed to a single high dose beam so as to minimize the effects of random beam variation and obtain a more homogenous distribution of pore size. Additionally, we will modify our design to include two nanoporous membrane filters in the lid so as to incorporate fault-tolerance. The flexibility of our approach also allows for further reduction of pore size if necessary.

The FLI intensities observed with the Xenogen IVIS system showed a strong positive correlation for cell numbers ranging from 10,000–100,000 cells, making it an indicator of viable cell number in that range. Instrument insensitivity restricts accurate measurements below this range. At lower cell numbers (≥2,500) a fluorescence plate reader which has higher sensitivity provided a positive correlation for a wider range of cell numbers.

A critical requirement for effective cell therapy is that the cellular graft be well oxygenated (Papas et al. 2000). To assess the survival and oxygenation of cells within our microcontainer, we engineered the rapid growing, highly metabolic 9L rat glioma cell line to constitutively express GFP and to bioluminesce in hypoxic conditions. FLI showed that fluorescent signal correlated strongly with cell number, suggesting that we can use FLI to score graft survival and function. FLI may also be used in the image-guided delivery of the cellular grafts.

Bioluminescent signal from cells in culture correlated with simulated hypoxia, indicating that BLI can be used to assess the oxygenation status of the cells, although basal signal was observed from cells maintained in normoxia. It is noteworthy that BLI signal from cells maintained under simulated hypoxia exceeded that from cells under normoxia even though cell numbers after 24 h exposure to $CoCl_2$ were lower than ‘normoxia’ controls, most likely owing to $CoCl_2$

toxicity (Wang et al. 2000). Fairly constant FLI/BLI signal ratio was observed within each group—'normoxia' and 'hypoxia'—but the ratio for 'hypoxia' was much less than 'normoxia' as expected. This is attributable to the increased BLI signal under 'hypoxia'. Owing to this differential in BLI signal in spite of fewer cells under simulated hypoxia, we expect that our 9L-3HRE-luc/GFP cells will be a more effective reporter of cell oxygenation in the absence of $CoCl_2$. The detection of BLI signal from a mere ~3,000 cells demonstrates the feasibility of using this method to obtain signal from small cellular grafts such as individual pancreatic islets. Our method can potentially be used for the *in vivo* evaluation of tissue-specific oxygenation of cellular grafts and may therefore aid in identifying suitable transplantation site.

For encapsulated cells, cells within non-porous micro-containers yielded significantly more bioluminescence signal than cells within nanoporous microcontainers after 48 h culture. These results indicate that the nanopores facilitated the oxygenation of encapsulated cells and that the 9L-3HRE-luc/GFP cells effectively scored the oxygenation of encapsulated cells. Although it is possible that some oxygen may have diffused through the male-female interface for both conditions, the signal differential between nanoporous and nonporous microcontainers clearly demonstrates the strength of this technique in evaluating the oxygenations status of cellular grafts. We observed basal signal from cells within the nanoporous microcontainers, while unencapsulated controls yielded no BLI signal for an equivalent time point and exposure. This result suggests that our nanopore array may not have fully oxygenated the encapsulated cells and that it may therefore be necessary to expand the nanopore array for this particular cell line and other highly metabolic ones. Although it is possible that the current nanopore configuration will adequately oxygenate less metabolic cell lines, we will extend our study to incorporate a denser nanopore array and create additional nanoporous surfaces on our microcontainer. In future studies, we will also explore strategies to ensure a hermetic seal at the interface of the lid and base of our microcontainer, and integrate radio frequency microsensors with the microcontainer so as to evaluate encapsulated cell function using MRI (Constantinidis et al. 2007; Gimi et al. 2003), which cannot be achieved with iron-oxide loaded microcapsules or metallic microcontainers, both of which result in signal loss and therefore can only reveal graft location and not graft function (Barnett et al. 2007; Evgenov et al. 2006; Gimi et al. 2005).

We have devised a nanoporous microcontainer for cell encapsulation and delivery, and have demonstrated a method for the creation of deep, anisotropic and uniform nanopores in SU-8 for application in cell based therapy. Our strategy for nanopore formation can be easily modified to accommodate the high throughput formation of nanostructures for other applications. Our method to assess the efficacy of nanopores in the oxygenation of cells can be adapted for other cell lines, and can be expanded to express reporter genes under stresses other than hypoxia.

Acknowledgments

We acknowledge NIH R01 EB007456 (BG). Optical imaging was facilitated by the SW-SAIR, which is supported in part by the NCI U24 CA 126608, the Simmons Cancer Center, and Department of Radiology at UT Southwestern Medical Center. The Caliper IVIS Spectrum was purchased with funds from an NCI Shared Instrumentation Grant SIO RR024757. The 9L glioma cells were a kind gift by Dr. Stephen Brown from the laboratory of Dr. Jae Ho Kim of Henry Ford Health System, Detroit, MI, USA. The 3HRE-tk-LUC vector was a kind gift from Dr. Richard K. Bruick from the laboratory of Dr. Steve McKnight of UT Southwestern Medical Center, Dallas, TX, USA. We thank Keith Bradshaw of UT Dallas for useful discussions.

References

Barnett BP, Arepally A, Karmarkar PV, Qian D, Gilson WD, Walczak P, Howland V, Lawler L, Lauzon C, Stuber M, Kraitchman DL, Bulte JW. Nat Med 2007;13:986. [PubMed: 17660829]

Bjerkvig R, Read TA, Vajkoczy P, Aebischer P, Pralong W, Platt S, Melvik JE, Hagen A, Dornish M. Acta Neurochir Suppl 2003;88:137. [PubMed: 14531571]

Burgos FJ, Gomez V, Pascual J, Marcen R, Villafruela JJ, Correa C, Cuevas B, Mampaso F, Garcia-Gonzalez R. Transplant Proc 2006;38:2585. [PubMed: 17098010]

Chicheportiche D, Reach G. Diabetologia 1988;31:54. [PubMed: 3280370]

Cho SH, Lu HM, Cauller L, Romero-Ortega MI, Lee JB, Hughes GA. Ieee Sensors Journal 2008;8:1830.

Constantinidis I, Grant SC, Celper S, Gauffin-Holmberg I, Agering K, Oca-Cossio JA, Bui JD, Flint J, Hamaty C, Simpson NE, Blackband SJ. Biomaterials 2007;28:2438. [PubMed: 17239948]

de Groot M, Schuurs TA, van Schilfgaarde R. J Surg Res 2004;121:141. [PubMed: 15313388]

Desai TA, Chu WH, Tu JK, Beattie GM, Hayek A, Ferrari M. Biotechnol Bioeng 1998;57:118. [PubMed: 10099185]

Evgenov NV, Medarova Z, Dai G, Bonner-Weir S, Moore A. Nat Med 2006;12:144. [PubMed: 16380717]

Gimi B, Eroglu S, Leoni L, Desai TA, Magin RL, Roman BB. Concepts Magn Reson B Magn Reson Eng 2003;18B:1.

Gimi B, Leong T, Gu Z, Yang M, Artemov D, Bhujwalla ZM, Gracias DH. Biomed Microdevices 2005;7:341. [PubMed: 16404512]

Gimi B, Kwon J, Kuznetsov A, Vachha B, Magin RL, Philipson LH, Lee JB. J Diabetes Sci Technol 2009;3:297. [PubMed: 19746206]

Hasse C, Bohrer T, Barth P, Stinner B, Cohen R, Cramer H, Zimmermann U, Rothmund M. World J Surg 2000;24:1361. [PubMed: 11038207]

Hortelano G, Al-Hendy A, Ofosu FA, Chang PL. Blood 1996;87:5095. [PubMed: 8652822]

Iwata H, Morikawa N, Fujii T, Takagi T, Samejima T, Ikada Y. Transplant Proc 1995;27:3224. [PubMed: 8539926]

Kin T, Rajotte RV, Dufour JM, Korbutt GS. Cell Transplant 2002;11:547. [PubMed: 12428744]

King A. Ups J Med Sci 2001;106:161. [PubMed: 12166508]

Papas KK, Long RC Jr, Constantinidis I, Sambanis A. Cell Transplant 2000;9:415. [PubMed: 10972340]

Rihova B. Adv Drug Deliv Rev 2000;42:65. [PubMed: 10942815]

Shapiro AM, Lakey JR, Ryan EA, Korbutt GS, Toth E, Warnock GL, Kneteman NM, Rajotte RV. N Engl J Med 2000;343:230. [PubMed: 10911004]

Thomlinson RH, Gray LH. Br J Cancer 1955;9:539. [PubMed: 13304213]

Tian H, McKnight SL, Russell DW. Genes Dev 1997;11:72. [PubMed: 9000051]

Vial T, Descotes J. Toxicology 2003;185:229. [PubMed: 12581698]

Visted T, Bjerkvig R, Enger PO. Neuro Oncol 2001;3:201. [PubMed: 11465401]

Voskerician G, Shive MS, Shawgo RS, von Recum H, Anderson JM, Cima MJ, Langer R. Biomaterials 2003;24:1959. [PubMed: 12615486]

Wang G, Hazra TK, Mitra S, Lee HM, Englander EW. Nucleic Acids Res 2000;28:2135. [PubMed: 10773083]

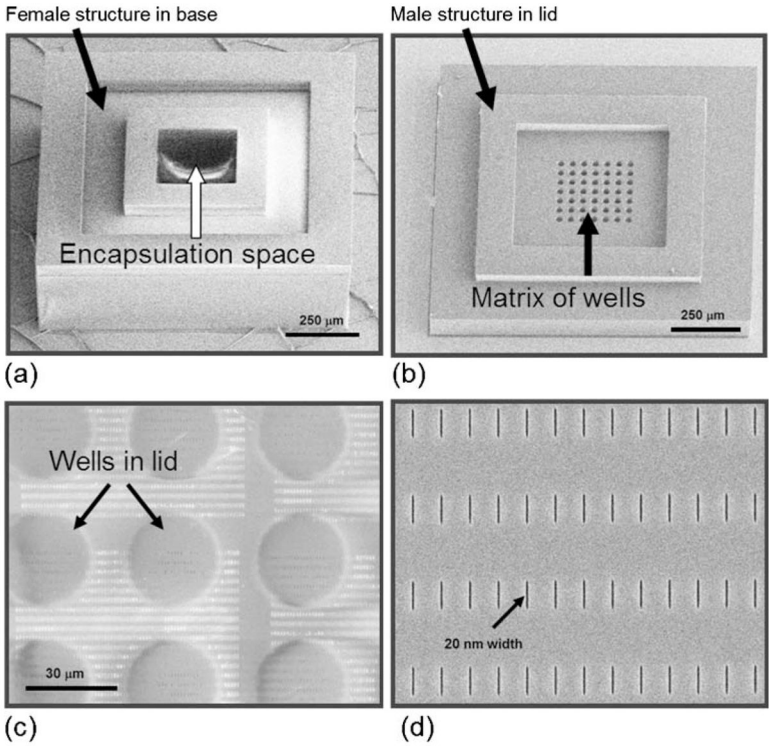

Fig. 1.

SEM images of the microcontainer's hollowed cubic base (**a**), and lid that contains a matrix of wells that exposes a thin nanoporous membrane at the base of the wells (**b**). The thin nanoporous membrane has a nanopore array which is shown magnified in panel (**c**). The nanopores (enlarged view, **d**) permit selective molecular transport through the membrane

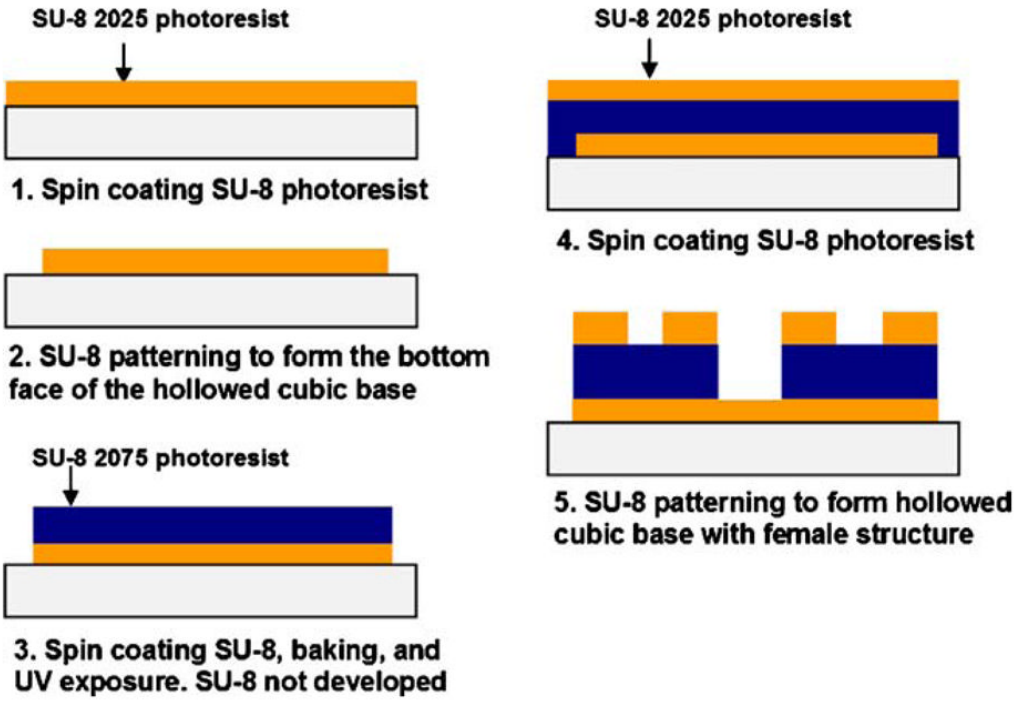

Fig. 2.
A schematic showing the fabrication sequence for the hollowed cubic base of the microcontainer

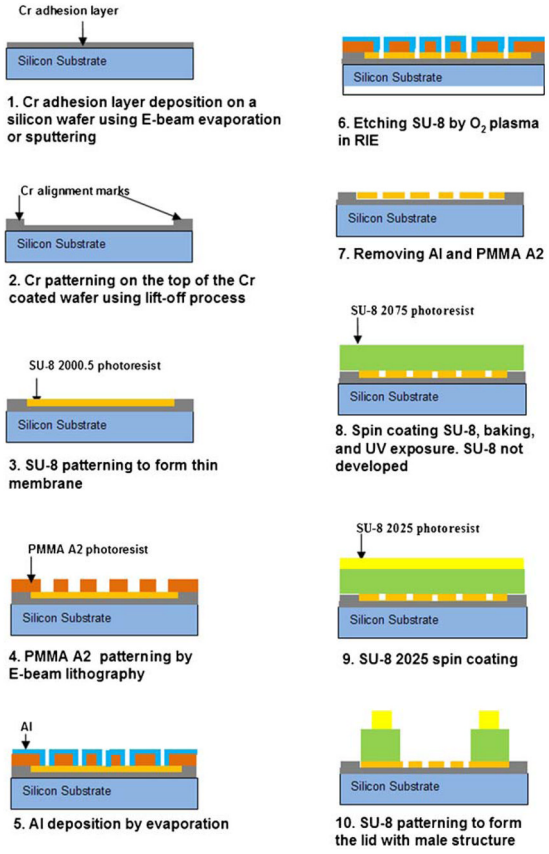

Fig. 3.
A schematic showing the fabrication sequence for the nanoporous lid of the microcontainer

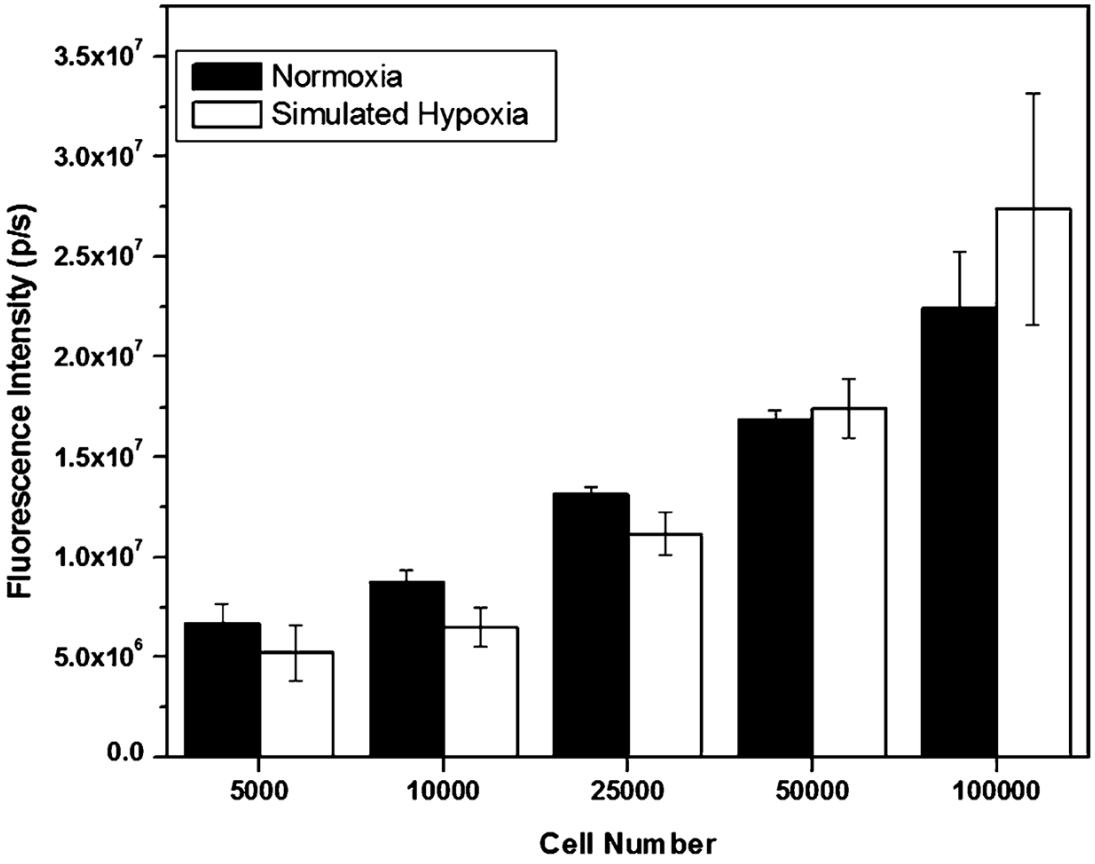

Fig. 4.
Fluorescence from cells maintained in normoxia and simulated hypoxia for 4 h

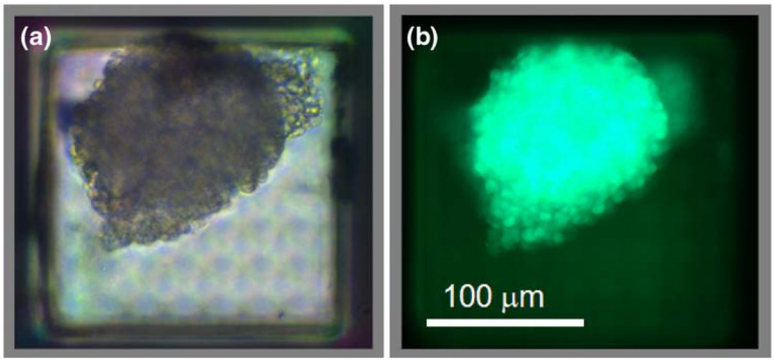

Fig. 5.

The transparent microcontainer was devised to facilitate optical imaging of the encapsulated cells. A representative phase contrast micrograph (**a**) and fluorescent image acquired in the green channel (**b**) of a cluster of ~3,000 9L-3HRE-luc/GFP cells encapsulated within the sealed microcontainer

Table 1

Fluorescence intensity versus cell number for 9L-3HRE-luc/GFP cells

Cell number	Fluorescence intensity (RFU)	Normalized fluorescence intensity (RFU/cell)
2,500	4.06E−01	1.65E−04
5,000	6.24E−01	1.25E−04
7,500	1.65E+00	2.20E−04
10,000	3.65E+00	3.65E−04
25,000	5.84E+00	2.34E−04
50,000	1.33E+01	2.66E−04
75,000	1.81E+01	2.41E−04
100,000	2.05E+01	2.05E−04